Appl. Phys. B 70 [Suppl.], S253–S259 (2000) / Digital Object Identifier (DOI) 10.1007/s003400000283

Applied Physics B
Lasers
and Optics

Mirror-dispersion-controlled OPA: a compact tool for sub-10-fs spectroscopy in the visible

G. Cerullo[1], M. Nisoli[1], S. Stagira[1], S. De Silvestri[1], G. Tempea[2], F. Krausz[2], K. Ferencz[3]

[1] Istituto Nazionale per la Fisica della Materia, CEQSE-CNR, Dipartimento di Fisica, Politecnico, 20133 Milano, Italy
(Fax: +39-02/2399-6126, E-mail: giulio.cerullo@fisi.polimi.it)
[2] Abteilung Quantenelektronik und Lasertechnik, Technische Universität Wien, 1040 Vienna, Austria
[3] Research Institute for Solid State Physics of the Hungarian Academy of Sciences, 1525 Budapest, Hungary

Received: 6 October 1999/Revised version: 12 February 2000/Published online: 24 May 2000 –

Abstract. We report on a sub-10-fs optical parametric amplifier in the visible, using noncollinear phase matching in β-barium borate, with a pulse compressor made exclusively of chirped dielectric mirrors. We employ mirrors of novel design, providing negative group delay dispersion for bandwidths of over 200 THz, up to the blue-green spectral region. The resulting setup, compact, easy to operate and reliable, is an ideal tool for ultrafast spectroscopy with extremely high time resolution. We use these pulses to observe in the time domain coherent oscillations in organic molecules with period as short as 16 fs.

PACS: 42.65.Re; 42.65.Yi; 42.79.Nv

Visible light pulses with sub-10-fs duration and μJ-level energy are required for several advanced ultrafast spectroscopy experiments, such as the study of extremely fast atomic and molecular dynamics, the generation of photon echoes, and the detection of coherent oscillations [1]. Until recently, the only available sources of such pulses have been dye lasers: by optical fiber compression of an amplified dye laser, pulses as short as 6 fs centered at 620 nm were generated [2], with energies of a few nJ; amplification of these pulses to the μJ level in a mixture of dyes was achieved at the expense of lengthening of the pulses to 16 fs [3]. Pulses as short as 13 fs with μJ-level energy were generated in the blue-green region by white-light continuum amplification in a mixture of dyes; a fraction of the energy of these pulses was then compressed to less than 10 fs [4]. Despite their good performance, the considerable complication and difficulty of operation of dye-laser-based systems prevented them from becoming workhorses in ultrafast spectroscopy. Since the development of Kerr lens mode-locking, femtosecond optical parametric amplifiers (OPAs) in the visible have become available [5–9]. These sources, despite their excellent stability and reliability, generated pulses longer than 50 fs because of the narrow phase-matching bandwidths obtainable in the collinear configuration. This limitation has been recently overcome thanks to the discovery of wavelength-independent phase-matching in β-barium borate (BBO) [10–12] when used for optical parametric generation (OPG): in a noncollinear geometry with a suitable pump-signal angle, in fact, the phase-matching angle becomes nearly independent of wavelength over a broad frequency range, thus allowing for ultrabroad amplification bandwidths.

Using this concept, non-collinear OPAs in the visible pumped by the second harmonic (SH) of an amplified Ti:sapphire laser were demonstrated by several groups. These systems provide amplified bandwidths in excess of 100 THz and pulse durations well below 10 fs, with μJ-level energy [13–19]). These OPA systems consist essentially of three components (see Fig. 1): a white light seed generation stage, a parametric gain stage and a pulse compressor. The most critical element is the pulse compressor, which must provide the required phase correction over broad bandwidths and guarantee high energy throughput. Up to

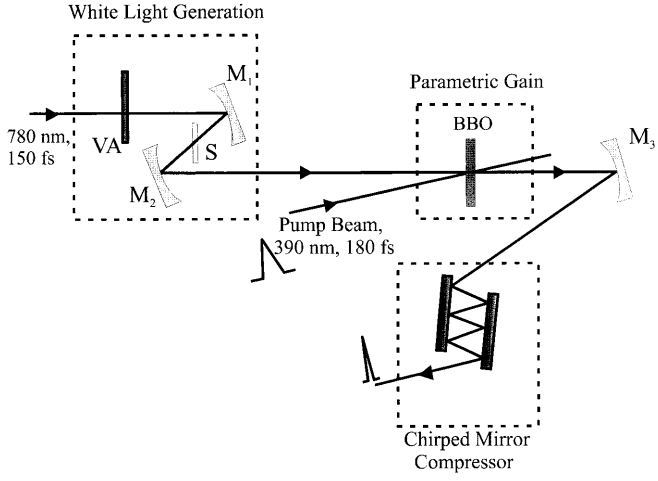

Fig. 1. Schematic of the noncollinear OPA and the chirped mirror pulse compressor. VA, variable optical density attenuator; S, 1-mm-thick sapphire plate; M_1, M_2, M_3, spherical mirrors

now several compressor schemes have been proposed, including Brewster-cut prisms [13, 14, 16, 17], thin-prism sequences [15], prism-grating [18], and prism-chirped mirror [19] combinations. The presence of prisms in all the configurations makes the compressor more sensitive to alignment, which increases the complexity of the system.

Chirped dielectric mirrors introduce a frequency-dependent group delay (GD) by reflecting different frequency components of the incident radiation at different positions within the multilayer structure [20, 21]. Until now chirped mirrors were designed to provide negative group delay dispersion (GDD) in the near-infrared and red spectral regions, for frequencies lower than 500 THz. Dispersion compensation using only chirped mirrors was previously demonstrated with laser oscillators [22], optical parametric oscillators [23], and pulse compressors [24, 25]. Besides enabling phase correction over broad bandwidths, this technique has the advantage of greatly simplifying the system design, allowing for compactness, reproducibility, and insensitivity to misalignment, which are of paramount importance in practical applications.

In this work we report on a noncollinear visible OPA system with a compressor made exclusively from chirped dielectric mirrors, providing negative GDD over the whole visible range, up to 600 THz (blue-green spectral region). These mirrors exploit a recently introduced design [26] which allows one to achieve GD that varies nearly linearly with frequency over bandwidths as broad as 200 THz. The resultant system is compact, easy to operate and reliable and generates sub-10-fs pulses in the visible spectral range: these characteristics make it an ideal tool for ultrafast spectroscopy with extremely high time resolution.

The paper is organized as follows. In Sect. 1, after briefly reviewing the properties of noncollinear phase matching in BBO, the experimental setup of the OPA is described in detail. In Sect. 2 we address the problem of pulse compression and present the results obtained using different kinds of chirped mirrors. In Sect. 3, to demonstrate the potentialities of the OPA system for ultrafast spectroscopy, we report on pump-probe experiments on different organic systems, featuring the direct time domain observation of extremely short-period molecular vibrations. Finally, in Sect. 4 we draw the conclusions and discuss the prospects for future work.

1 The noncollinear ultrabroadband OPA

Before discussing the OPA experimental setup, let us briefly review the properties of noncollinear phase matching in BBO. In OPG the interacting beams must satisfy the energy conservation condition $\omega_p = \omega_s + \omega_i$ and the momentum conservation (phase matching) condition $\boldsymbol{k}_p = \boldsymbol{k}_s + \boldsymbol{k}_i$ (p, s, and i stand for pump, signal, and idler beams, respectively). Phase matching is usually achieved by suitably orienting the nonlinear crystal. Figure 2 shows, for type I ($o + o \rightarrow e$) OPG in BBO and a pump wavelength of 400 nm, the phase-matching angle θ as a function of signal wavelength. For a collinear configuration (dash-dotted line for $\alpha = 0°$ in Fig. 2) θ strongly depends on the signal wavelength so that, for a given crystal orientation, phase matching can be achieved only over a narrow signal frequency range. In a noncollinear configuration the wavelength dependence of θ becomes weaker until, for a pump-signal angle $\alpha = 3.7°$, a given crystal orientation ($\theta = 32°$) allows us to achieve phase matching over most of the visible range. Fortuitously, this angle is also very close to the angle ($\approx 4°$) for which spatial walkoff between pump and signal is compensated, thus providing high gain. This favourable property was first discovered by Gale et al. [10–12] and exploited to build broadband optical parametric oscillators and OPAs.

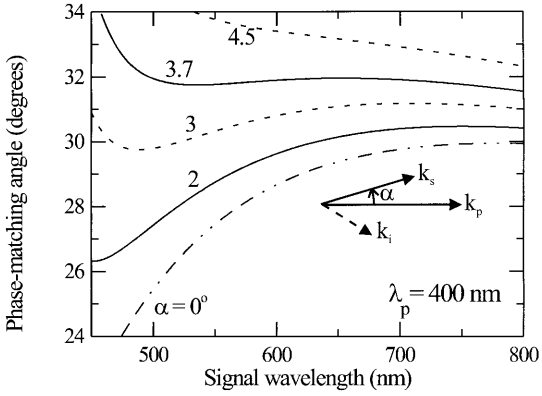

Fig. 2. Phase-matching curves for a noncollinear type I BBO OPA pumped at 400 nm, as a function of the pump-signal angle α; $\boldsymbol{k}_p$, $\boldsymbol{k}_s$, and $\boldsymbol{k}_i$ are the pump, signal, and idler wavevectors, respectively

A schematic of the experimental setup of the noncollinear OPA used in this work is shown in Fig. 1. We start with an amplified Ti:sapphire laser (Clark-MXR Model CPA-1) generating 150-fs pulses at 780 nm and 1-kHz repetition rate with energy of as much as 750 μJ. The pump pulses (390 nm wavelength, 10 μJ energy) are obtained by frequency doubling a fraction of the light in a 1-mm-thick lithium triborate crystal. Owing to group-velocity mismatch in the second-harmonic generation process, the pump pulses are slightly broadened to ≈ 180 fs when they reach the OPA. The seed pulses are generated by focusing a fraction of the 780-nm beam, with energy of approximately 2 μJ, into a 1-mm-thick sapphire plate. By carefully controlling the energy incident on the plate (with the help of a variable-optical-density attenuator) and the position of the plate around the focus, a highly stable single-filament white light continuum is generated [5–7]. The group delay of the visible portion of the white light, measured with the technique of optical Kerr gating [14], is small and fairly linear with frequency. To avoid the introduction of additional chirp, we employ reflective optics to guide the white light to the amplification stage. The tilting angles of the spherical mirrors are kept as small as possible (less than 4°), so that the resulting astigmatism is negligible.

Parametric gain is achieved in a 1-mm-thick BBO crystal, cut at $\theta = 32°$, using type I phase-matching. The crystal length is close to the pulse-splitting length for signal and pump in the wavelength range of interest; a single-pass configuration is employed in order to increase the gain bandwidth. To minimize self-focusing effects, the BBO crystal is positioned slightly beyond the focus of the pump beam. At the crystal position, the spot size of the pump beam is approximately 120 μm, corresponding to an intensity of 120 GW/cm^2; at higher intensities distortions and beam breakup are observed. The white-light seed is imaged by spherical mirror M_2 in the BBO crystal, with a spot size nearly matching that of the pump beam. The amplified pulses have energy of approximately 2 μJ, peak-to-peak fluctuations

of less than 7% and maintain a TEM_{00} beam quality. After the gain stage the amplified beam is collimated by spherical mirror M_3 and sent to the chirped-mirror compressor. The compressed pulses are then directed to a balanced noncollinear autocorrelator, employing silver mirrors and a 20-μm-thick BBO crystal.

As previously demonstrated, the bandwidth of the amplified pulses strongly depends on the alignment of the BBO crystal and on the pump-seed angle. When the BBO crystal is aligned perpendicular to the pump beam and is illuminated by the pump pulse, it emits a strong off-axis parametric superfluorescence in the visible in a cone with an apex angle of 6.4°([27, 28], see inset of Fig. 3a); this is the direction for which group-velocity matching between signal and idler is guaranteed. If the pump-signal angle is carefully adjusted to match the cone apex angle and the optimum pump-seed delay is set, an ultrabroad gain bandwidth, extending over most of the visible, is observed. A typical amplified pulse spectrum obtained under these conditions, measured with a calibrated optical multichannel analyzer, is shown in Fig. 3a: it displays a FWHM of 180 THz.

Due to the use of reflecting optics in the system and of a thin sapphire plate, the chirp of the amplified pulses is relatively low. The group delay of the ultrabroadband amplified pulses was measured by upconversion with a 10-nm spectral slice of the pulse, selected with an interference filter and having approximately 70 fs FWHM duration. After the upconverting crystal, an UV monochromator allowed us to determine the relative arrival times of different frequency components of the pulse. The measurement (see points in Fig. 3b) yields an overall group delay of ≈ 500 fs between the red and the blue components of the spectrum. The experimental curve can be reproduced quite accurately (see solid line in Fig. 3b) by taking into account the group delays introduced by the sapphire plate, the BBO crystal, the 1-mm-thick BK7 beam splitter used in the autocorrelator, and the path (≈ 3.5 m) in air.

2 Pulse compression using chirped mirrors

The ultrabroadband visible chirped mirror system (VIS-CM) [29] used for these experiments was designed by a semi-analytical method. A simple formula permits a starting structure to be determined that leads to the required GD and reflectance characteristics after limited computer optimization. Because the bandwidth constitutes an input parameter in the procedure, the design of the ultrabroadband mirrors becomes straightforward. The VIS-CM provides high reflectivity ($R > 99\%$; see dashed line in Fig. 4a) over a range of almost 200 THz and an average GDD of $-28\,\mathrm{fs}^2$ with fluctuations of $\pm 14\,\mathrm{fs}^2$. In Fig. 4a we plot as a solid line the calculated GD vs. frequency relationship and as squares the

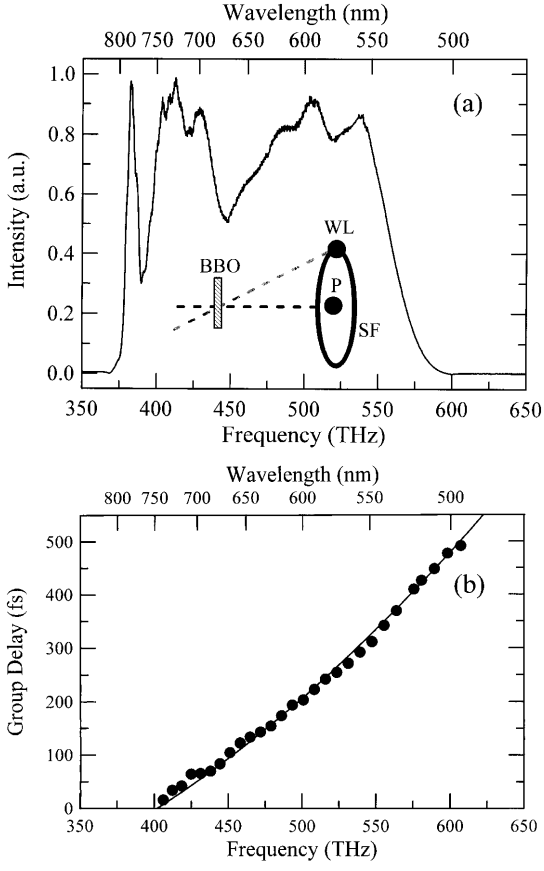

Fig. 3. a Amplified pulse spectrum obtained under optimum alignment conditions. The pump-seed angle matches the apex angle of the superfluorescence cone, as shown in the *inset*: WL, white-light seed; P, pump beam; SF, superfluorescence ring. **b** *Points*: measured GD of the amplified pulses vs. frequency; *solid line*, calculated GD vs. frequency

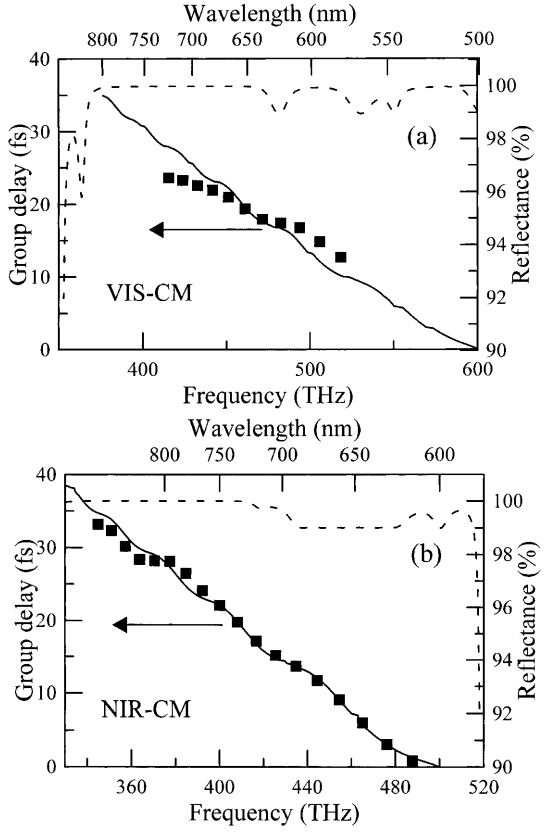

Fig. 4. a *Dashed* (*solid*) *line*: calculated reflectance (GD) vs. frequency for the chirped mirror design VIS-CM. *Full squares*: experimental data obtained by white light interferometry, the absolute value of the group delay being arbitrarily chosen. **b** Same as (**a**), but for NIR-CM

experimental data, measured with a white-light interferometer [30]. The differences between theoretical and experimental data can be attributed to imperfect knowledge of the coating material dispersion at short wavelengths. We believe that these are the first chirped mirrors to provide negative GDD in the 500–600 THz frequency range: the mirrors used in the research reported in [19], in fact, have negative GDD only for frequencies lower than 500 THz, and for higher frequencies phase correction required the use of prisms. The performance of the VIS-CM was compared, in the red spectral region, with that of existing mirror systems designed for hollow-fiber pulse compressors [25] and working in the near-infrared spectral region (NIR-CM). The characteristics of these mirrors, which provide an average GDD of $-40\,\mathrm{fs}^2$ from 350 to 500 THz, are shown in Fig. 4b.

The GD required from the compressor (which is the opposite of the GD of the amplified pulses) is shown Fig. 5 as a solid line: we can see that, over the full gain bandwidth of the OPA, its frequency dependence notably deviates from a linear behavior, because of third-order dispersion introduced by the optical elements. The curve is however fairly linear over bandwidths of the order of 100 THz, so it can be reproduced by a sufficient number of bounces on the chirped mirrors. As shown in Fig. 5, good matching in the blue and in the red can be achieved by use of, respectively, 17 and 13 bounces on the VIS-CM; in the red spectral range, similar results can be obtained with only 7 bounces on the NIR-CM. Therefore, being unable to provide the required phase correction over the whole pulse bandwidth, we chose to use a pump-seed angle slightly smaller than the optimum, thus reducing the amplified bandwidth: in this case, the OPA could be tuned by varying the pump-seed delay or slightly tilting the BBO crystal. Typical red and blue-green amplified pulse spectra obtained in this configuration are shown in Fig. 6.

Experimentally, optimum compression of the blue-green pulses (spectrum (a) of Fig. 6) was achieved with 18 bounces on the VIS-CM: the autocorrelation (Fig. 7a) yields a FWHM pulse duration of 9.5 fs, assuming a sech^2 pulse shape, to be compared with 8.5 fs obtained from a Fourier transform of the pulse spectrum. The red pulses (spectrum (b) of Fig. 6) could be compressed to 8.5-fs duration after 14 bounces on a VIS-CM (solid curve in Fig. 7b): in this case the transform-limited pulse duration was 6.5 fs. For this wavelength range,

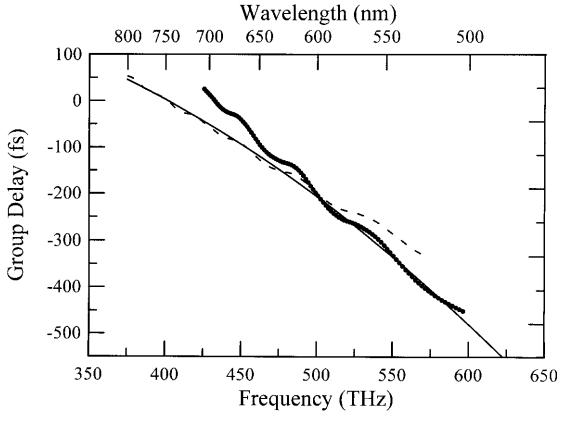

Fig. 5. *Solid line*: desired GD of the compressor (opposite of the GD of the amplified pulses) vs. frequency; *dashed line* (*points*), GD after 17(13) bounces on VIS-CM

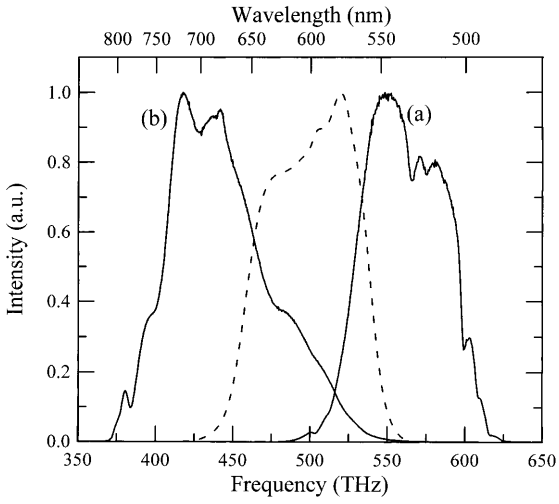

Fig. 6. Amplified pulse spectra obtained with a pump-seed angle slightly smaller than the optimum value. Tuning is achieved by slightly tilting the BBO crystal or varying the pump-seed delay

better results were obtained with the NIR-CM, and a pulse duration of 7.5 fs was measured after 7 bounces (dashed curve in Fig. 7b). The experimental number of bounces is in good agreement with that expected from the theoretical GD calculations. The measured pulse widths are quite close to the transform-limited values, indicating the high quality of the compressor, and were easily reproducible on a day-to-day basis without any compressor adjustment. The chirped-mirror compressor therefore adds reliability as well as compactness to the system and considerably simplifies its operation in real-world and ultrafast spectroscopy experiments.

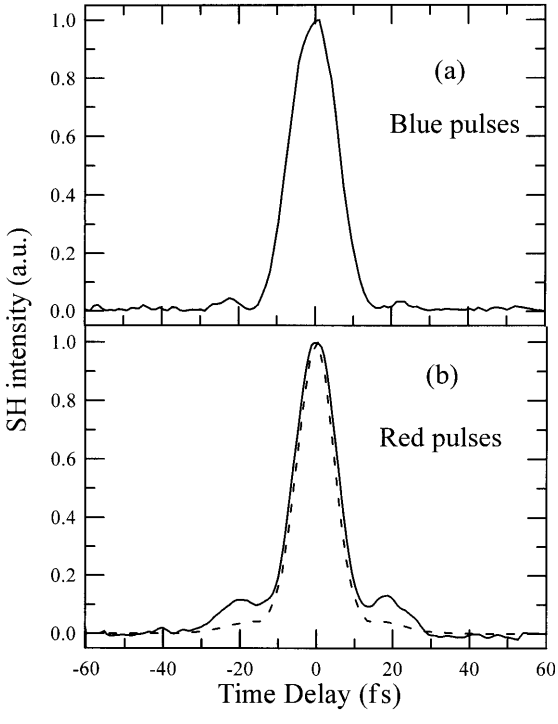

Fig. 7a,b. Autocorrelation traces of **a** the compressed blue pulses and **b** the compressed red pulses for a VIS-CM (*solid curves*) and a NIR-CM (*dashed curve*). SH, second harmonic

3 Applications to ultrafast spectroscopy

The system described in this work was used extensively for ultrafast spectroscopy measurements with extremely high resolution: any additional dispersion met downstream the OPA, such as for example from cuvette windows, could be easily compensated for by increasing the number of bounces on the chirped mirrors. Here, to demonstrate the potentialities of the system and the quality of the achievable data, we briefly show some results obtained with two π-conjugated organic materials: α-sexithienyl (T_6) and polydiacetylene (PDA).

T_6 is an important model compound for understanding the photophysics of conjugated polymers [31] and in addition it is a promising material for molecular electronics applications [32]. In T_6, like in most linear conjugated systems, the first electronic transition ($\pi \rightarrow \pi^*$ transition) is strongly coupled to a few normal modes of the carbon backbone, having the right symmetry to induce dimerization. The direct observation of these modes is highly relevant for the understanding of excited state relaxation in these materials and of their linear and nonlinear optical properties. The vibronic spectra obtained with traditional techniques are in general quite complex and their assignment presents ambiguities due to the dramatic influence of broadening effects and the presence of traps and molecular defects. Vibronic coupling can be studied directly in the time domain if the material is excited with a light pulse sufficiently short compared with the periods of the coupled vibrations. This technique, known as impulsive coherent vibrational spectroscopy, provides unique spectral and dynamical information on the optically coupled modes.

In our experiments, polycrystalline T_6 films with an approximate thickness of 100 nm are resonantly excited by a blue pulse and probed by a delayed and attenuated replica of the pulse [33]. After the sample, single wavelengths of the broadband probe pulse are selected using 10-nm-bandwidth interference filters. Figure 8 shows the differential transmission (ΔT) signal vs pump-probe delay at the probe wavelength of 510 nm; features at negative and near-zero delays are due to pump-perturbed free induction decay and coherent coupling [34]. For positive delays we observe a negative ΔT signal, due to photoinduced absorption originating from the Frenkel exciton level [35]. The signal is modulated by a complex oscillatory pattern, caused by the motion of the wave packet launched by the pump pulse on the multidimensional excited state potential energy surface (PES) [36]. The inset of Fig. 8 shows the Fourier transform of the oscillatory component of the signal, after a slowly varying background has been subtracted. We clearly identify five modes, at frequencies $\omega_1 = 112\,\mathrm{cm}^{-1}$, $\omega_2 = 299\,\mathrm{cm}^{-1}$, $\omega_3 = 702\,\mathrm{cm}^{-1}$, $\omega_4 = 1040\,\mathrm{cm}^{-1}$, $\omega_5 = 1454\,\mathrm{cm}^{-1}$, respectively. At other probe wavelengths, the ΔT signal is modulated by an oscillatory pattern due to the same five characteristic frequencies, although with different relative intensities. These data allow us to unambiguously determine for the first time the vibronic structure in T_6; in addition, they provide important information on the PES characteristics. As an example we show in Fig. 9 the Fourier transforms of the oscillatory component of the signal in Fig. 8 performed on two separate time windows, 0–500 fs and 500–1000 fs: we observe a clear shift of the ω_5 mode to higher frequencies as the time delay increases. The time evolution is better depicted in the inset of Fig. 9, showing the peak of the Fourier transform of 300-fs blocks of the signal, each shifted by 50 fs, as a function of time delay. To understand this result, we recall that the period of the ω_5 mode is short enough to cause sizable displacement of the polarization wave packet on the excited state PES during pump excitation. It is thus possible, by a second interaction with the pump field, to bring the wave packet down to the ground state, well out of the equilibrium position corresponding to the PES minimum. We thus generate vibrational wave packets both within the ground state and the excited state PES. A possible explanation of the frequency change could be anharmonicity of the ground state PES associated with wavepacket relaxation. Another possibility is that ground and excited state wavepackets oscillate with slightly different frequencies (with the higher frequency corresponding to the ground state) and have different damping times. The faster damping of the lower frequency motion would give rise to an apparent frequency shift. In this case, a longer damping time would correspond to the ground state motion, in agreement with the previous observation of longer damping times of ground state os-

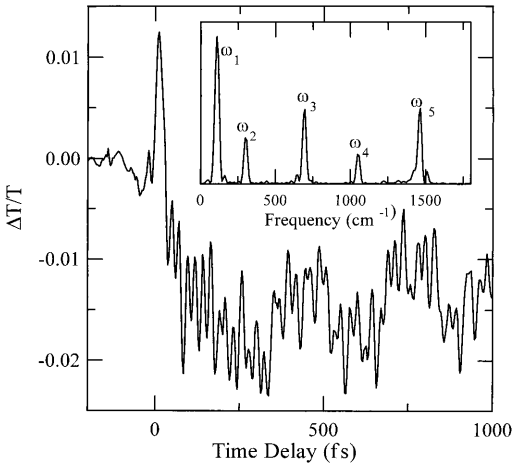

Fig. 8. Differential transmission vs. pump-probe delay for a film of T_6 pumped by an ultrashort blue pulse. After the sample, the probe pulse is spectrally filtered using an interference filter centered at 510 nm. *Inset*: Fourier transform of the oscillatory component of the signal

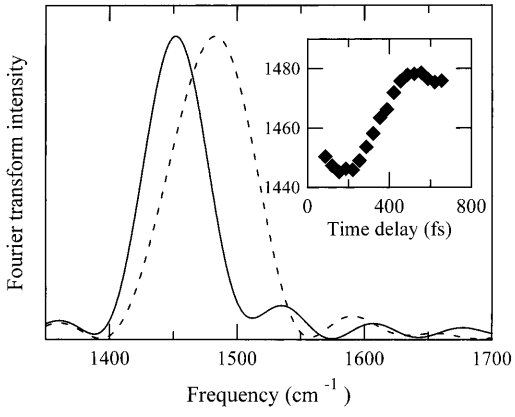

Fig. 9. Fourier transform of the oscillatory component of the signal in Fig. 8 for the time windows 0–500 fs (*solid line*) and 500–1000 fs (*dashed line*); the *inset* shows the peak frequency of 300-fs blocks of the signal as a function of time delay

cillations when probing on the blue side of the absorption spectrum [37].

PDA is a conjugated polymer with an alternance of single, double, and triple bonds, showing large delocalization and small $\pi - \pi^*$ gap. It can be used to produce very high quality optical waveguides and is the most promising organic material for third-order nonlinear optical applications [38–40]. We performed experiments on blends of poly[1,6-bis(3, 6-didhexadecyl-N-carbazolyl)-2,4-hexadiyne] (polyDCDH-HS) and polyethylene. The sub-10-fs excitation pulse was centered at 540 nm, close to the peak of ground state absorption. In Fig. 10 we show the ΔT signal, at the probe wavelength of 600 nm, as a function of pump-probe delay. We observe an increased transmission, assigned to bleaching of the optical transition, strongly modulated by an oscillatory pattern, due to coupling of the optical transition to the C=C (frequency 1500 cm^{-1}, period 22 fs) and C≡C (frequency 2100 cm^{-1}, period 16 fs) vibrational modes. The C≡C stretching mode, which has a period of approximately 16 fs, is to our knowledge the highest frequency molecular oscillation directly observed in the time domain.

Additional insight on the molecular evolution following photoexcitation can be gained by performing a sliding-window Fourier transform (spectrogram) of the oscillatory component of the signal, defined as [41]

$$F(\nu, \tau) = \int_0^\infty f(t)h(t-\tau)\exp(-\mathrm{j}2\pi\nu t)\mathrm{d}t\,,$$

where $h(t) = \exp(-t^2/t_0^2)$ is a Gaussian window function; the spectrogram combines temporal and spectral information and allows us to follow the temporal evolution of the oscillation frequencies. A spectrogram for the data in Fig. 10 is reported in Fig. 11. This analysis shows that initially the vibrational spectrum is dominated by the C=C mode, whereas the C≡C mode becomes strongly coupled to the electronic transition only ≈ 150 fs after the excitation. This result strongly supports the hypothesis that photoexcitation gives rise to a transient butadrienic configuration (with the C=C mode dominant) which is quickly followed (within ≈ 150 fs) by the return to a stable acetylenic configuration (C≡C mode dominant). These data provide new insight into the early-time photophysics of polydiacetylene after photoexcitation and show the potential of our spectroscopic system for investigating real-time evolution of the geometric structure of molecules.

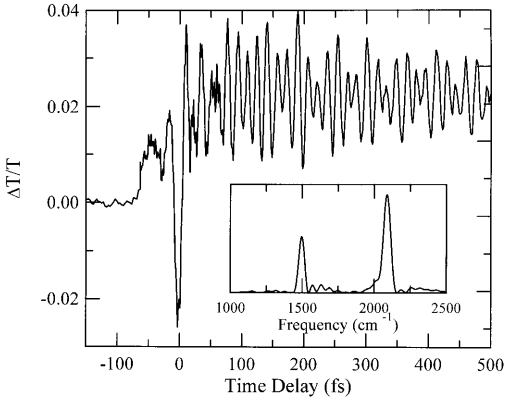

Fig. 10. Differential transmission vs. pump-probe delay for a film of polydiacetylene pumped by an ultrashort blue pulse. After the sample, the probe pulse is spectrally filtered using a 10-nm interference filter centered at 600 nm. *Inset*: Fourier transform of the oscillatory component of the signal

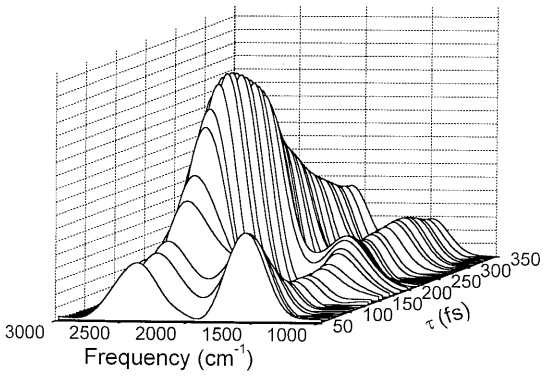

Fig. 11. Sliding-window Fourier transform of the oscillatory component of the signal in Fig. 10

4 Conclusion

We have developed a compact visible OPA system with a dispersive delay line using exclusively chirped mirrors. We have employed what we believe are the first ultrabroadband visible chirped mirrors, providing negative GDD up to 600 THz (blue-green spectral region). The use of the chirped mirrors considerably simplifies the compression stage and allows us to generate sub-10-fs pulses consistently and reliably. The performance and the ease of operation of this system make it an ideal tool for ultrafast spectroscopy with very high time resolution. Visible light pulses allow us to resonantly excite a number of materials of interest in physics, chemistry, and biology. To demonstrate the potential of the system and the quality of the obtainable data, we have presented pump-probe experiments on conjugated organic materials. We are able to directly observe in the time domain coherent molecular oscillations with periods as short as 16 fs.

The mirrors that we used for this research are designed to correct for second-order dispersion and are able to provide phase correction for the amplified pulses only over bandwidths of ≈ 100 THz. This work provides further stimulus for the development of ultrabroadband chirped mirrors including also third-order dispersion compensation. Such mirrors will be able to provide the required phase correction over the entire gain bandwidth of the OPA, which will allow us to generate transform-limited pulses with a bandwidth spanning most of the visible range.

References

1. T. Elsaesser, J.G. Fujimoto, D.A. Wiersma, W. Zinth (Eds.): *Ultrafast Phenomena XI* (Springer, Berlin, Heidelberg 1998)
2. R.L. Fork, C.H. Brito-Cruz, P.C. Becker, C.V. Shank: Opt. Lett. **12**, 483 (1987)
3. G. Boyer, M. Franco, J.P. Chambaret, A. Migus, A. Antonetti, P. Georges, F. Salin, A. Brun: Appl. Phys. Lett. **53**, 823 (1998)
4. R.W. Schoenlein, J.-Y. Bigot, M.T. Portella, C.V. Shank: Appl. Phys. Lett. **58**, 801 (1991)
5. M.K. Reed, M.K. Steiner-Shepard, D. Negus: Opt. Lett. **19**, 1855 (1994)

6. M.K. Reed, M.S. Armas, M.K. Steiner-Shepard, D. Negus: Opt. Lett. **20**, 605 (1994)
7. M.K. Reed, M.K. Steiner-Shepard, M.S. Armas, D. Negus: J. Opt. Soc. Am. B **12**, 2229 (1995)
8. S.R. Greenfield, M.R. Wasielewski: Opt. Lett. **20**, 1394 (1995)
9. P. Di Trapani, A. Andreoni, C. Solcia, P. Foggi, R. Danielius, A. Dubietis, A. Piskarkas: J. Opt. Soc. Am. B **12**, 2237 (1995)
10. T.J. Driscoll, G.M. Gale, F. Hache: Opt. Commun. **110**, 368 (1994)
11. G.M. Gale, M. Cavallari, T.J. Driscoll, F. Hache: Opt. Lett. **20**, 1562 (1995)
12. G.M. Gale, F. Hache, M. Cavallari: IEEE J. Sel. Top. Quantum Electron. **4**, 224 (1998)
13. T. Wilhelm, J. Piel, E. Riedle: Opt. Lett. **22**, 1494 (1997)
14. G. Cerullo, M. Nisoli, S. De Silvestri: Appl. Phys. Lett. **71**, 3616 (1997)
15. G. Cerullo, M. Nisoli, S. Stagira, S. De Silvestri: Opt. Lett. **23**, 1283 (1998)
16. A. Shirakawa, T. Kobayashi: Appl. Phys. Lett. **72**, 147 (1998)
17. A. Shirakawa, T. Kobayashi: IEICE Trans. Electron. **E81-C**, 246 (1998)
18. A. Shirakawa, I. Sakane, T. Kobayashi: Opt. Lett. **23**, 1292 (1998)
19. A. Shirakawa, I. Sakane, M. Takasaka, T. Kobayashi: Appl. Phys. Lett. **74**, 2268 (1999)
20. R. Szipöcs, K. Ferenc, C. Spielmann, F. Krausz: Opt. Lett. **19**, 201 (1994)
21. F.X. Kärtner, N. Matuschek, T. Schibli, U. Keller, H.A. Haus, C. Heine, R. Morf, V. Scheuer, M. Tilsch, T. Tschudi: Opt. Lett. **22**, 831 (1997)
22. A. Stingl, Ch. Spielmann, F. Krausz, R. Szipocz: Opt. Lett. **19**, 204 (1994)
23. J. Hebling, E.J. Mayer, J. Kuhl, R. Szipocz: Opt. Lett. **20**, 919 (1995)
24. R. Szipocz, A. Köhazi-Kis: Appl. Phys. B **65**, 115 (1997)
25. S. Sartania, Z. Cheng, M. Lenzner, G. Tempea, Ch. Spielmann, F. Krausz, K. Ferencz: Opt. Lett. **22**, 522 (1997)
26. G. Tempea, F. Krausz, Ch. Spielmann, K. Ferencz: IEEE J. Sel. Top. Quantum Electron. **4**, 193 (1998)
27. R. Danielius, A. Piskarkas, P. Di Trapani, A. Andreoni, C. Solcia, P. Foggi: Opt. Lett. **21**, 973 (1996)
28. V. Krylov, O. Ollikainen, J. Gallus, U. Wild, A. Rebane, A. Kalintsev: Opt. Lett. **23**, 100 (1998)
29. G. Cerullo, M. Nisoli, S. Stagira, S. De Silvestri, G. Tempea, F. Krausz, K. Ferencz: Opt. Lett. **24**, 1529 (1999)
30. W.H. Knox, M.N. Pearson, K.D. Li, C.A. Hirlimann: Opt. Lett. **13**, 574 (1988)
31. C. Taliani, L.M. Blinov: Adv. Mater. **8**, 353 (1996)
32. A. Dodabalapur, L. Torsi, H.E. Katz: Science **268**, 270 (1995)
33. G. Cerullo, G. Lanzani, M. Muccini, C. Taliani, S. De Silvestri: Phys. Rev. Lett. **83**, 231 (1999)
34. C.H. Brito Cruz, et al.: IEEE J. Quantum Electron. **QE-24**, 261 (1988)
35. G. Lanzani, et al.: Phys. Rev. Lett. **79**, 3066 (1997)
36. S. Mukamel: *Principles Of Nonlinear Optical Spectroscopy* (Oxford University Press, New York 1995)
37. C.J. Bardeen, Q. Wang, C.V. Shank: J. Phys. Chem. A **102**, 2759 (1998)
38. T. Kobayashi (Ed.): *Relaxation in Polymers* (World Scientific, Singapore 1993)
39. T.-A. Pham, A. Daunois, J.-C. Merle, J. Le Moigne, J.-Y. Bigot: Phys. Rev. Lett. **74**, 904 (1995)
40. J-Y. Bigot, T.-A. Pham, T. Barisien: Chem. Phys. Lett. **259**, 469 (1996)
41. M.J.J. Vrakking, D.M. Villeneuve, D.M. Stolow: Phys. Rev. A **54**, 37 (1996)